ORIGINAL ARTICLE

3D characterization of pores in the cortical bone of human femur in the elderly at different locations as determined by synchrotron micro-computed tomography images

C. Chappard · S. Bensalah · C. Olivier ·
P. J. Gouttenoire · A. Marchadier · C. Benhamou ·
F. Peyrin

Abstract

Summary Diaphysis, inferior, and lateral superior regions of the femoral neck are subjected to diverse mechanical loads. Using micro-CT based on synchrotron radiation, three-dimensional morphology and connectivity of the pore network are location dependent, underlying different remodeling mechanisms.

Introduction The three-dimensional (3D) morphology and connectivity of the pore network at various locations in human femurs subjected to diverse mechanical loads were assessed using micro-CT based on synchrotron radiation.

Methods The cortex from 20 human femurs (mean age, 78.3±12.4 years) was taken from the diaphysis (D), the inferior (IN), and the lateral superior (LS) regions of the femoral neck. The voxel size of the 3D reconstructed image was 7.5 μm. Cortical thickness and pore volume/tissue volume (Po.V/TV), pore diameter (Po.Dm) and spacing (Po.Sp) were determined. The pore surface/pore volume ratio (Po.S/Po.V), the number of pores (Po.N), the degrees of anisotropy (DA), and the connectivity density (ConnD), the degree of mineralization (DMB) were also determined.

Results The characteristics of the pore network in femoral cortical bone were found to be location dependent. There was greater porosity, Po.Dm, and Po.N, and more large (180–270 μm), extra-large (270–360 μm) and giant pores (>360 μm) in the LS compared to the IN and D. The difference in porosity in between the periosteal and endosteal layers was mostly due to an increase of Po.Dm rather than Po.N. There was a lower DMB of bone in the LS, which is consistent with a higher remodeling rate.

Conclusion The results provide evidence for large variations in the structure of the internal pore network in cortical bone. These variations could involve different underlying remodeling mechanisms.

Introduction

The analysis of bone structure is crucial in understanding the physiopathology of osteoporosis, which is an important health problem. Hip fracture is recognized as the most serious osteoporotic fracture because of the high medical costs and the high mortality and morbidity involved [1]. In the femoral neck, the cortical shell contributes 40–90 % of the bending rigidity [2]. However, compared to trabecular bone, there are very few studies on cortical bone. For a number of years, microstructural variations were assessed by two-dimensional (2D) histological methods, while porosity was assessed by physical methods. With these methods, it was shown that microstructural variations had a significant impact on the material properties of cortical bone [3–6]. By analogy with trabecular bone (composed of a trabecular network), cortical bone is composed of a pore network and possesses a complex and dynamic microstructure that cannot be fully characterized with 2D analytical

C. Chappard (✉)
UMR 7052 cnrs-Paris Diderot, PRES Sorbonne Paris Cité, B2OA,
Paris, France
e-mail: christine.chappard@inserm.fr

S. Bensalah
ENIT, U2S,
Tunis, Tunisia

C. Olivier · P. J. Gouttenoire · F. Peyrin
ESRF, ID19,
Grenoble, France

A. Marchadier · C. Benhamou
Inserm, U658,
Orleans, France

methods [7]. More recently, it became possible to characterize the spatial arrangement of the pore network by micro-computed tomography (micro-CT), which has become a quasi-standard tool for the examination of trabecular bone in three dimensions (3D) with isotropic resolution. This technique can also be used to study cortical bone [8]. Indeed, micro-CT based on synchrotron radiation (SR) has been used to characterize the neurovascular pore arrangement in the cortical bone of the inferior neck of the femur [9] and in a single femur [10], but it is not widely available; in contrast, desktop micro-CT with conventional X-rays has been used more frequently [11–16].

The parameters used to characterize the spatial arrangement of cortical pores were pore diameter (Po.Dm), pore number (Po.N), pore separation (Po.Sp) and the specific surface organization of pores (Po.S/Po.V) in the cortical femur [11–16]. Estimation of the connectivity based on a skeletonization technique was proposed by Cooper at al [12, 13].

The high variability in the diameter (ranging from 50 to 450 μm) and the shape of the neurovascular pores in cortical bone was reported previously [13–17]. The differences in size and shape are the result of modeling and remodeling processes. Indeed, porous spaces occur in primary osteons formed by modeling; the initial destruction of the cylindrical packets is followed by the circumferential deposition of new bony lamellae. This remodeling process creates the Haversian system (secondary osteons), which is surrounded by a cement line [18]. The Haversian canals run parallel to the surface of the bone cortex, and the Volkmann canals are connected perpendicularly to the Haversian canals. Both Haversian and Volkmann canals are predominantly located in the external (periosteal) region of the cortex, and large resorption cavities created by several cycles of remodeling are predominantly located near the internal (endosteal) region.

The tension and shear fracture toughness of the femoral neck are greater than those of the femoral shaft [19]. The femoral neck is different from the femoral shaft in terms of microstructure and composition and their relationship to fracture toughness [6]. Cortical bone has been describe to carry 30 % of the load in the subcapital region, 50 % in the mid-neck, 96 % at the base of the neck, and 80 % at the intertrochanteric region [20]. There are also differences between the inferior cortex of the neck or calcar femorale (the principal loading sector of the cortex during walking), which experiences compressive forces, and the supero-lateral cortex of the neck, which experiences a lower level of tension loading from the hip musculature [21].

Due to high photon flux and the monochromaticity of the X-ray beams extracted from the synchrotron light, SR micro-CT has many advantages compared to conventional micro-CT. This allows for the evaluation of local mineralization [12] with a high signal-to-noise ratio and without beam hardening; moreover, reconstruction avoids the creation of cone-beam artifacts due to its parallel-beam geometry [23].

The 3D arrangement of pores in different regions of the femur submitted to different loading forces has not yet been examined. The aim of the present study was to assess the 3D morphology and connectivity of the pore network at various locations along the human femur that are subject to different mechanical loads, using micro-CT-based synchrotron radiation as a tool.

Materials and methods

Specimens

The cadaveric right femurs from 20 Caucasian subjects were harvested within 10 days of death at the Pathology Institute, Rene Descartes University, Paris, France. Collection of these human tissue specimens was conducted according to pertinent protocols established by the Human Ethics Committee of Inserm.

Fourteen femurs were from females (mean age, 79.3 ± 14.6 years; range, 53–97 years), and six were from males (mean age, 76 ± 4.4 years; range, 72–83 years). No data were available regarding the cause of death, previous illnesses, or the medical treatment of these individuals. The femurs did not present obvious pathology, except for those with fractures, which were eliminated. The soft tissues around femurs were removed, and the femurs were enclosed in plastic bags at -20 °C.

Sixty samples of cortical bone were cut transversally using a low-speed diamond saw (Isomet 1000®, Buehler, Germany). Twenty samples from the diaphysis were harvested from the medial femoral shaft 2 cm below the lesser trochanter. Twenty samples were harvested from the inferior neck in the calcar femorale and from the lateral superior area of the femoral neck close to the subcapital region (superior neck). The location where samples were harvested is illustrated in Fig. 1. The cortex was taken at full thickness and a 12-mm height.

Image acquisition

Fifty-five bone cores were imaged using the SR micro-CT at the European Synchrotron Radiation Facility (ESRF; Grenoble). Forty-five bone cores were from 15 subjects; three sites were imaged in each core. Only two sites were imaged for the remaining five subjects (diaphysis + inferior neck for two, diaphysis + superior neck for two, and inferior neck + superior neck for one). SR micro-CT images were obtained from the 3D parallel-beam SR micro-CT setup
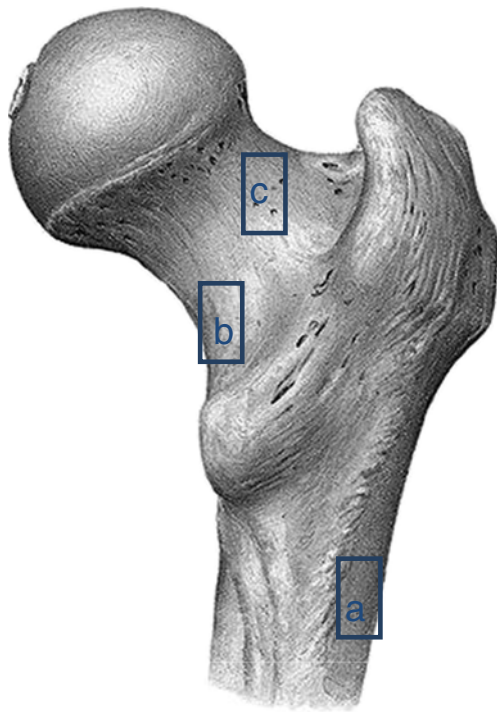
Fig. 1 Locations where the specimens were harvested from the femurs: *a* diaphysis, *b* inferior neck, *c* superior neck

developed on beamline ID 19 at the ESRF. A detailed description of the device was previously reported [24].

The samples were positioned to obtain 2D projection images perpendicular to the Haversian system.

The setup used a very intense, homogeneous, parallel, and monochromatic beam. The transmitted X-ray beam was recorded with a scintillator coupled to a 2D 2,048×2,048 charge coupled device camera with a dynamic range of 14 bits. The optical system was set to obtain a pixel size of 7.5 μm (in order to cover the field of view of the samples examined). Due to the size of the largest samples, the energy setting used was 30 keV. To optimize the quality of each reconstructed image, 3,500 views were regularly acquired over a total angular range of 360°. Dark current and reference images (without the sample) were regularly taken during the data acquisition period and were used for flat-field correction. The exposure time for each radiograph was 0.3 s. The total acquisition time, including all mechanical operations and image recording and transmission, was approximately 30 min. The 3D images were reconstructed from the set of 2D radiographic projections using tomographic reconstruction based on filtered back-projections. The size of the cubic voxel in the reconstructed images was 7.5 μm.

Typical 2D and 3D renderings of micro-CT images from the same subject, acquired with SR at different locations, are illustrated in Fig. 2. All samples were imaged from the outer margin to the endosteal region. Three sites were available for only 15 of the subjects tested in the present study.
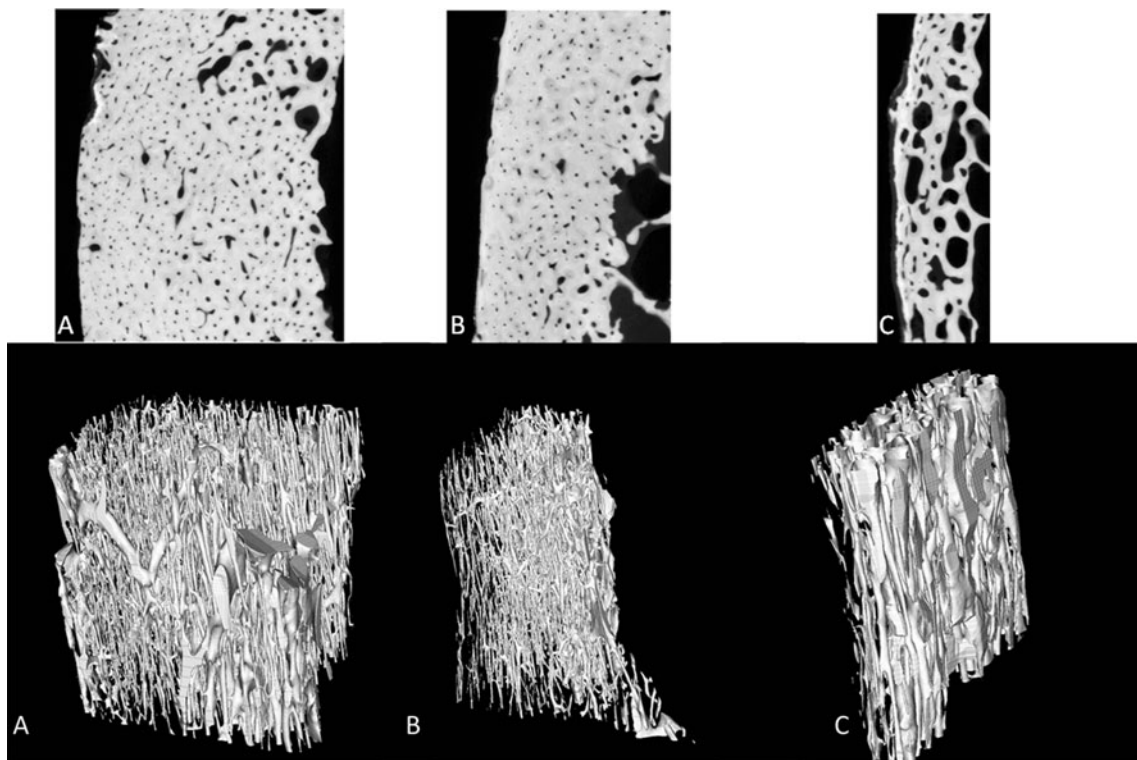
Fig. 2 Two-dimensional and 3D images from the same individual. Resolution, 7.5 μm^3. **a** Diaphysis. **b** Inferior neck. **c** Superior neck. The periosteal areas in the specimens are shown at the *right*

Image processing

In each sample, a total volume of interest (VOI) of 5 mm in height was selected to extend through the entire thickness of cortical bone from the periosteum to the endosteum. The endosteal border was identified when both irregular interconnected voids and non-osteonal structures were encountered. This VOI selection was performed using a semi-automatic procedure based on manual contouring on a selected number of slices, followed by interpolation. A periosteal sub-VOI 1-mm thick and an endosteal sub-VOI corresponding to the remaining thickness of the cortical ring were also defined for each bone sample (see Fig. 3).

The histograms of the 3D reconstructed volumes were composed of two peaks, corresponding to bone and voids, respectively. Because all images were acquired in the same conditions, an identical global threshold was used for all images, above which all voxels were considered as bone and below which all voxels were considered as voids. The threshold is approximately the average of the mean values of the two peaks from the entire data set and corresponded to a linear attenuation coefficient of 1.31 cm^{-1} at 30 keV. Calculations were performed in terms of pixels attributed to voids instead of matter.

Measured and calculated parameters

The cortical thickness was measured directly and manually on the image, corresponding to the minimal distance between periosteal and endosteal borders using CtAn® Skyscan software. The total volume corresponds to 642 slices, and the measurements were performed every 30 slices. We therefore had 22 measurements for each sample; the average distance was considered for all future measurements. Morphological parameters were also calculated using the CtAn® Skyscan software. All pores (primary and secondary osteonal pores) within the scanned images were included in these calculations.

The pore volume/tissue volume (Po.V/TV) corresponds to the void proportion. The pore diameter (Po.Dm, μm) and

pore spacing (Po.Sp, μm) were measured with the model-independent method described by Hildebrand and Rüegsegger [25]. The pore surface (Po.S, per square millimeter) was obtained by triangulation of the surface of the mineralized bone phase. The pore volume (Po.V) was calculated using tetrahedrons corresponding to the enclosed volume of triangulated surfaces [26]. The pore number (Po.N, per millimeter) was defined as the inverse of the mean distance between the middle axes of the structure [27]; these axes were identified by a skeletonization process.

The degree of anisotropy (DA; no unit), defining the orientation of the pore structure, was evaluated by fitting the mean intercept length (MIL) points to an ellipsoid [28]. When the largest (smallest) is denoted as MIL1 (MIL3), then DA is defined as:

$$DA = MIL1/MIL3 \tag{1}$$

DA equals 1 for isotropic structures and is larger than 1 for anisotropic structures. The higher the DA value, the more anisotropic the structure is.

The connectivity was quantified by the Euler characteristic (χ) using a proprietary procedure according to the method described in detail by Odgaard for quantifying aspects of bone architecture [29]. The Euler characteristic may be directly estimated from the 3D array of voxels using the following decomposition:

$$\chi = n_0 - n_1 + n_2 - n_3 \tag{2}$$

where n_0, n_1, n_2, and n_3 are, respectively, the number of vertices, edges, faces, and voxels. If the object is made of a single connected component and contains no voids, the Euler number is simply related to the connectivity β_1 by:

$$\chi = 1 - \beta_1 \tag{3}$$

The connectivity is defined as the maximum number of branches that may be cut without separating the structure [30]. A high value means a highly connected network.

Fig. 3 Examples of "volume of interest" selection by manual contouring followed by an interpolation to keep track of the contours of the cortical bone

Original image+ total VOI

total VOI   periosteal VOI   endosteal VOI
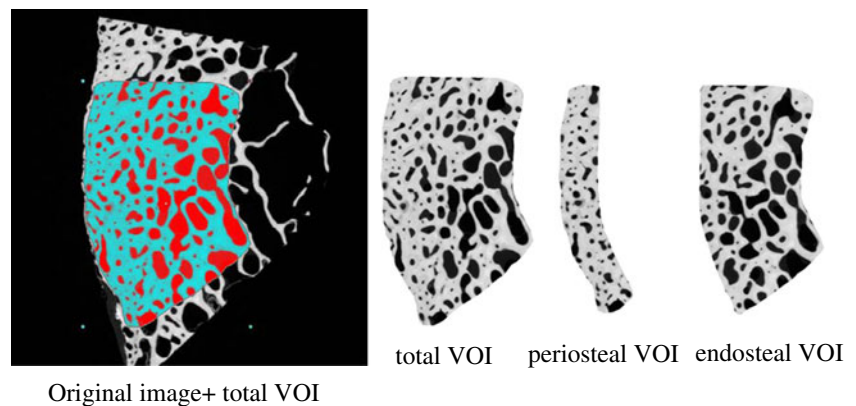
The connectivity characteristic was normalized by the total volume of each VOI; for this reason, the connectivity density (ConnD) was expressed in per cubic millimeter.

The images provided by SR micro-CT are assumed to be quantitative maps of the linear attenuation coefficient of bone tissue at 30 keV. The data were converted to obtain the degree of bone mineralization (DMB), which was defined as the local hydroxyapatite (HA) concentration in the tissue examined. The method exploits the theoretical relationship between the measured linear attenuation coefficient (μ) and concentration of HA as described in our previous work [22]. By calculating the mass attenuation coefficient of HA and water at 30 keV, which were found to be 2.099 and 0.3756 g/cm^3, respectively, the conversion between DMB and μ is given by:

$$DMB = (\mu - 0.3756)/1.929 \qquad (4)$$

Data analyses

Descriptive statistics were computed for all numerical parameter data. All statistical computations were performed using NCSS (2004, Kaysville, UT). A Shapiro–Wilkinson test was used to check the normality of the distribution of parameters. An ANOVA was used to compare the location groups (inferior neck, superior neck, diaphysis). In the event of a non-normal distribution, a Kruskal–Wallis test was performed. Multiple comparison analysis was performed using the Newman–Keuls test. Correlations between pore network parameters were performed with Spearman correlation coefficients (ρ) within the total VOIs. Po.Dm distributions were compared between sites using a Kruskal–Wallis test followed by a Tukey–Kramer post-hoc test. A paired T-test was used to compare periosteal and endosteal VOIs; a Wilcoxon test was used for non-normal data distributions. For the degree of mineralization data, comparisons were made by means of an ANOVA with a missing data procedure followed by the Newman–Keuls post-hoc test [31].

Results

The results for the 3D microarchitectural parameters obtained from bone specimens from the same individual at different cortical sites, namely the diaphysis and inferior and superior parts of the femoral neck, are compared in Table 1. The cortical thickness differed statistically across sites. The diaphysis thickness was greater than the cortical thickness of the femoral neck, and the inferior neck thickness was greater than that of the superior neck. Po.V/TV, Po.N, and Po.Sp were significantly different with higher porosity and Po.N values at the superior neck and lower Po.Sp values

Table 1 Values of 3D microarchitectural parameters of various cortical regions in human femur from the same individual

	Cortical thickness (mm)	Po.V/TV (%)	Po.S/Po.V (1/mm)	Po.Dm (µm)	Po.N (1/mm)	Po.Sp (µm)	ConnD (1/mm^3)	DA
Inferior neck	2.92±1.0	11.2±7.9	52.4±29.1	165±79	0.63±0.26	354±86	39±28.6	4.7±1.7
	2.82 (0.82–4.32)	8.6 (2.8–30.4)	45.1 (21.1–116.6)	156 (70–338)	0.54 (0.35–1.11)	348 (267–623)	35.5 (4.9–110)	4.6 (1.3–7.3)
Superior neck	1.01±0.44	26.3±12.3	29.2±7.9	219±64	1.20±0.52	273±64	44.6±24.9	6.4±5.5
	1.0 (0.35–1.81)	24.2 (5.1–45.8)	28.0 (17.3–48.7)	204 (130–315)	1.07 (0.40–2.53)	246 (199–444)	41.0 (13.4–93.2)	4.6 (2.7–20.1)
Diaphysis	4.58±1.24	11.1±8.1	49.2±28.0	168.8±98.7	0.64±0.23	333±44	30.4±28.2	3.9±0.8
	4.66 (1.16–6.13)	10.0 (1.7–40.6)	40.8 (14.2–105.6)	144 (60–397)	0.60 (0.26–1.00)	321 (255–403)	18.7 (7.9–98.1)	3.7 (2.6–5.3)
ANOVA	<10^{-4}	7.10^{-4}	0.02	ns	0.001	0.002	ns	ns
Post-hoc test	sup/inf/diaph	sup/inf-diaph	sup/inf		sup/inf-diaph	sup/inf-diaph		

Sexes were pooled ($n=15$). Statistical comparisons were performed using ANOVA and, in the event of non-normality, using the Kruskal–Wallis test (results in italics). Multiple comparisons were made using the Newman–Keuls post-hoc test. In regular font, mean±SD. In italics, median (min–max)

ns not significant

compared to corresponding values from the inferior neck and diaphysis. The specific surface of the pore (Po.S/Po.V) was significantly lower at the superior neck compared to the inferior neck.

Table 2 presents the matrix of correlation coefficients for the Total VOIs. The porosity was highly correlated with Po.Sp and Po.N in the superior neck and highly correlated with Po.Dm and Po.N in the inferior neck and diaphysis. The connD derived from the Euler number correlated only with Po.N in the superior neck.

Table 3 presents differences in parameters between periosteal and endosteal VOIs at both the diaphysis and inferior neck. Po.V/TV and Po.Dm parameters were statistically lower in the periosteal VOIs at both the inferior neck and diaphysis sites. The Po.S/Po.V parameter was statistically higher in the periosteal VOIs in the inferior neck as well as the diaphysis. The Po.N parameter was statistically lower in the periosteal VOIs at the inferior neck, and the mean DA was lower only in the diaphysis, whereas the mean Po.Sp was similar in both sites. Between the periosteal and endosteal layers, the differences in porosity in the inferior neck and diaphysis were +152 and +87 %, respectively, whereas the respective differences in Po.Dm were +61 and +50 %; for Po.N, these differences were −43 and −17 %.

Figure 4 shows the percentage distribution of the Po.Dm values classified into five groups: small (7–95 μm), intermediate (95–180 μm), large (180–270 μm), extra-large (270–360 μm), and giant pores (>360 μm). Pores with diameters of 7–95 μm correspond to primary or secondary osteons, and pores with diameters >360 μm correspond to remodeling cavities. Figure 4a shows the distribution of the Po.Dm values at various sites in the periosteal VOIs. Small pores were significantly more frequent in the diaphysis and inferior neck than in the superior neck. Large and extra-large pores were significantly more frequent in the superior neck than in the diaphysis and inferior neck; in the case of giant pores, the difference was observed only in the diaphysis. Figure 4b shows the comparison between the periosteal and endosteal sites at the inferior neck and diaphysis. The present study provided evidence that small pores were significantly more frequent in the periosteal areas of bone specimens at both sites, whereas giant and extra-large pores were more frequent at the endosteal sites. Pores of intermediate size were significantly more frequent in the endosteal area of the inferior neck. When comparing the diaphysis and inferior neck, there was no difference between periosteal and endosteal values.

The mean DMB±SD was 1.03±0.03, 1.02±0.05, and 0.97±0.03 g/cm^3 for the inferior neck, diaphysis, and superior neck, respectively ($p=3.10^{-4}$), with the superior neck values being significantly different from the others according to the post-hoc test.

Table 2 Matrix of Spearman correlation coefficients [for the indicated relationships] between different micro-architectural parameters within the total VOIs

	Cortical thickness	Po.V/TV (%)	Po.S/Po.V (1/mm)	Po.Dm (μm)	Po.N (1/mm)	Po.Sp (μm)	DA	ConnD (1/mm³)
Cortical thickness	1							
Po.V/TV (%)	−0.82*/−0.47**/ns	1						
Po.S/Po.V (1/mm)	ns/0.52**/ns	−0.77*/−0.82*/−0.94***	1					
Po.Dm (μm)	ns/ns/ns	0.51*/0.86*/0.93*	−0.83*/−0.89*/−0.97*	1				
Po.N (1/mm)	−0.72*/ns/ns	0.83*/0.83*/0.89*	ns/0.55**/−0.75***	ns/0.51**/0.71***	1			
Po.Sp (μm)	0.67*/ns/ns	−0.83*/−0.51/−0.58*	ns/ns/ns	ns/ns/ns	−0.85*/−0.63***/−0.66***	1		
DA	−0.51**/ns/−0.46**	ns/ns/0.57**	ns/ns/ns	ns/ns/ns	ns/ns/ns	ns/ns/ns	1	
ConnD (1/mm³)	ns/ns/ns	ns/ns/ns	ns/ns/ns	ns/ns/ns	0.53**/ns/ns	ns/ns/ns	ns/ns/ns	1

The correlation coefficients from the supero-external region of the neck, the inferior neck, and the diaphysis are presented from left to right

*p<0.001; **p>0.05; ***p<0.01

Table 3 Values for the micro-structural parameters in the periosteal (1-mm thick) and endosteal layers in the same specimen ($n=15$)

	% Periosteal area	Po.V/TV (%)	Po.S/Po.V (1/mm)	Po.Dm (µm)	Po.N (1/mm)	Po.Sp (µm)	DA
Inferior neck							
Periosteal VOI	32.3±6.9	6.1±5.6	76.9±39.4	132±111	0.44±0.17	338±44	3.6±1.4
	32.4 (23.1–43.8)	*4.3 (0.8–20.2)*	*69.2 (15.2–131.3)*	*89 (49–406)*	*0.45 (0.16–0.76)*	*339 (265–430)*	*3.0 (1.9–7.3)*
Endosteal VOI		15.4±15.7	45.8±27.1	213±175	0.63±0.22	332±35	3.3±0.6
		7.6 (2.3–53.0)	*43.6 (8.3–99.8)*	*159 (71–634)*	*0.59 (0.30–1.03)*	*330 (260–388)*	*3.2 (2.2–4.4)*
p		*0.0007*	*<10⁻⁴*	*0.0006*	0.002	ns	ns
Diaphysis							
Periosteal VOI	25.6±17.1	7.3±6.7	72.7±36.0	105±51	0.59±0.28	315±44	2.8±1.7
	21.4 (12.7–86.2)	*5.0 (1.2–20.6)*	*67.1 (14.9–139.4)*	*88 (44–207)*	*0.44 (0.25–1.0)*	*309 (226–395)*	*2.5 (1.4–8.3)*
Endosteal VOI		13.7±11.4	45.7±27.9	158±119	0.69±0.26	366±126	3.8 ±0.8
		12.3 (1.9–37.4)	*39.2 (13.8–102.5)*	*142 (63–420)*	*0.73 (0.25–1.15)*	*317 (218–701)*	*3.7 (2.8–5.9)*
p		0.00002	*<10⁻⁴*	*0.0005*	ns	ns	*0.002*

Comparisons were performed by the paired T-test; the non-parametric Wilcoxon test was used for non-normal data (in italics). In regular font, mean ±SD. In italics, median (min–max)

Discussion

General observations

The present study is the first to provide a 3D analysis of the internal macro-porosity of cortical bone at different locations with widely variable load-bearing capacity. For this purpose, micro-CT imaging by SR was implemented. The high quality of the images obtained facilitated the identification of the difference in internal structure. The 7.5-µm resolution of the images did not allow observation of the micro-porosity of the microscopic canaliculi or osteocyte lacunae. A previous study showed that spatial resolution higher than 10 µm is necessary to obtain consistent porosity data [32]. This condition was fulfilled in our study because we used a voxel size of 7.5 µm to obtain the entire cortical thickness, because when the resolution increases, the field of view decreases [33].

In a recent review, it was suggested that there is a progressive increase in the complexity of the porous network with advanced age when pores undergo a process of coalescence related to the remodeling activity [34], but the variability of the porosity microstructure as correlated with a particular site is not known. In our study, the pore network characteristics of femoral cortical bone depended on their specific location: Porosity and Po.N values obtained from the superior region of the femoral neck were greater than those found in the diaphysis and inferior neck. These data show that the cortex has higher porosity in tension than in compression [35].

Compared to results obtained from the inferior neck and diaphysis, large, extra-large, and giant pores were observed more frequently in the superior part of the femoral neck. Small pores (mostly corresponding to primary or secondary

osteons) were more often present in the periosteal area; giant pores (corresponding to resorption cavities) were found in the endosteal area of the inferior neck and diaphysis. However, it was not possible to clearly distinguish in the SR images whether pores were surrounded by primary or secondary osteons without clearly identifiable cement lines. At 1.4-µm resolution, Cooper et al. showed that it was possible to enhance the images of cement lines by creating a Z-projection with adjacent frames [10].

Porosity has been reported to be the main determinant of cortical bone tensile strength. Mac Calden et al. reported that changes in porosity account for 76 % of the reduction in bone strength [5]. The present study provides evidence that the relationship between porosity, Po.N. Po.Dm, and Po.Sp is dependent on site location. At the superior neck, in contrast to other sites, the porosity is higher with a variability that is weakly dependent on Po.Dm. In the specimens examined in the present study, there were more giant and extra-large pores within the superior femoral neck compared to the inferior neck and diaphysis. The superior neck, which is a load-bearing zone experiencing a low level of tension from forces generated by the hip musculature, shows very high remodeling activity, with resorption predominating, leading to a high numbers of pores and, to a lesser extent, large cavities, which probably correspond to the earliest stages of trabecularization. In contrast, the inferior neck, which is a compressive load-bearing zone, shows low remodeling activity with few pores; most of the pores present are small.

Both tensile and shear fracture toughness decrease significantly with increasing porosity [6]. The greater fracture toughness in the femoral neck cannot be explained in our case by a difference in porosity because the inferior neck and diaphysis have similar levels

Fig. 4 The distribution of pore diameters, grouped according to size, in the 15 individuals tested. Pores 7–95 microns in diameter correspond to primary osteons, and pores with a diameter >360 microns correspond to remodeling cavities. **a** Comparison of total VOIs among the three sites (diaphysis, inferior neck, and supero-external neck). The Kruskal–Wallis test was used in conjunction with the Tukey–Kramer post-hoc test for multiple comparisons. ¥a, significant difference between the supero-external neck and diaphysis (p<.01); ¥b, significant difference between the superior neck and either the diaphysis or inferior neck (p<0.01). **b** Comparison between the periosteal and endosteal VOIs of the diaphysis and inferior neck. *p<0.05; ¥ p<0.01 by the Wilcoxon test
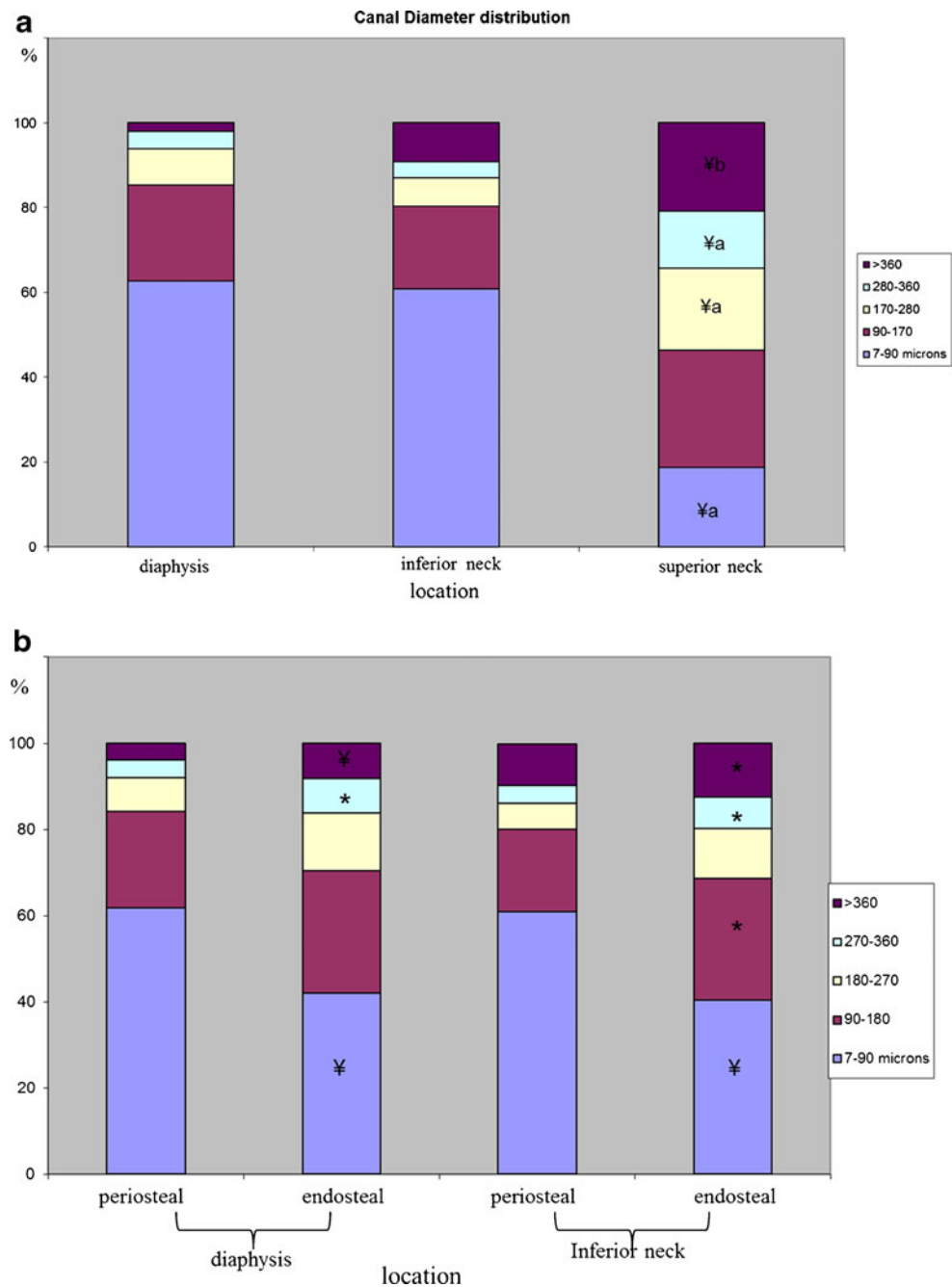
of porosity. In contrast, the gradient of porosity and Po.N between periosteal area and endosteal are greater in inferior neck than in diaphysis.

Diaphysis

The present study showed a median porosity of 12 % in the diaphysis with a median pore diameter of 144 μm. Using conventional X-ray micro-CT, Cooper et al. reported a mean porosity of 7.3 % at the mid-femoral shaft in a subject population of men and women with a large age range (from 18 to 92 years old) [13]. Stein et al. used histomorphometry techniques on a large population of 96 subjects and reported a median porosity of 5.9 % in the mid-diaphysis. They also reported a gain in porosity of 0.03 %/year with age. The older subjects, when compared to younger individuals, were more likely to exhibit large pore diameters than higher pore numbers [36]. In our study, the upper shafts rather than the mid-shaft were studied, which partly explained the variation in porosity in addition to differences in the methods used for measurement.

In other studies reported in the literature, the average diameter of porous structures in the human femoral shaft bone ranged from approximately 30 μm for the Haversian pores to

300–400 μm for resorption spaces [11, 37]. Accordingly, the pores were classified by size to individualize the Haversian canals of resorption lacunae; the pores less than 90 μm in size are most certainly from Haversian canals, and pores greater than 360 μm in size are most likely to occur in resorption lacunae.

In the present study, the porosity of the diaphysis was represented by both Po.Dm and by the Po.N as a progressive increase in Po.Dm from the periosteal to the endosteal regions. These results are concordant with a previous 3D analysis of the mid-femoral shaft using conventional micro-CT; the increase in PoV/TV was identified as a product of an increase of Po.Dm rather than an increase in Po.N [13]. The internal gradient of Po.Dm is consistent with most studies performed at the femoral diaphysis [37–39]. Giant pores are considered to be the result of excessive resorption and are responsible at the endosteal border for trabecularization of the cortex and for cortical thinning [37–39]. It is known that the basic multicellular unit preferentially remodels bone close to the endosteum and rarely near the periosteum [38]. More recently, microradiographs performed at the mid-shaft, femoral neck, and 1 cm below the great trochanter were used to demonstrate that cortical thinning resulted from the coalescence of intracortical pores [17].

Femoral neck

The present study compared the results from the femoral neck, which is a frequent fracture site, and the diaphysis. Moreover, the fracture toughness of the femoral neck has been found to differ from that of the femoral shaft [6]. The femoral neck has a less cellular and more mineralized periosteum than the femoral diaphyseal bone [40], with a consequent difference in the quality of bone apposition at this site. Cortical thickness is known to be at its minimum value in the superior part of the femoral neck and at its maximum value in the inferior part [21]. The results of the present study indicate pronounced internal pore network structure heterogeneity between the superior and inferior regions of the neck. Yeni et al. did not find differences in porosity or in pore area between the inferior neck and posterior neck [6]. Our samples were harvested near the subcapital region, which could explain the difference. In another study, a significant gradient in porosity from the inferior cortex to the superior cortex of the femoral neck was found in females and in some males using histomorphometric methods [35]. The increased porosity associated with lower cortical thickness could explain the difference between the inferior neck and superior neck in load-bearing capacity [20].

Using SR micro-CT images (voxel size, 10 μm), Bousson et al. obtained a porosity of 15.88 % at the inferior neck location in an older female population with a mean age of 86.9 years [9]. Compared to our results, the difference in terms of porosity is probably due to the age (10 years older) and gender (female) of the respective subjects. The discrepancy in results could also be partly due to the voxel size used. The variability of results in relation to voxel size was already highlighted by Cooper and coworkers, who reported a 25 % increase in the porosity measurement when the voxel size was varied from 5 to 10 μm [14]. In Chen's study, the porosity ranged from 5 to 12.7 % and was related to gender and age (57 to 98 years) [16]. The results of the present study are near the upper limit of theirs albeit with an appreciable number of protocol differences. First, those authors used conventional X-ray techniques, which could create potential beam-hardening artifacts leading to apparent heterogeneities. It has been demonstrated that volumes measured with conventional micro-CT are underestimated compared to those estimated using SR micro-CT in trabecular bone [23]. The same phenomenon probably occurs in cortical bone. Secondly, the thresholding process is also a potential source of erroneous results because this step has already been identified by Cooper et al. as a critical problem with conventional micro-CT images [14]. In Chen's study, a single threshold was used for the entire data set. Because there are smaller differences between gray levels corresponding to pores and bone in conventional micro-CT compared to SR micro-CT [23], a single threshold may yield inaccurate results when used for a few samples. For this reason, Cooper et al. used a manually adjustable threshold for each sample; they argued that variations in X-ray attenuation are problematic when using a global threshold [14]. However, a single threshold has been recommended for comparisons between different groups [41]. In the present study, there was no ambiguity in relation to the gray levels of solid bone or pores in the SR micro-CT images. The use of a global standardized threshold was thus possible because of the large differences between gray levels corresponding to bone and pores.

Pore distribution between periosteal and endosteal areas

For both the inferior neck and diaphysis, small pores corresponding to primary or secondary osteons were mostly present in the 1-mm periosteal area; giant pores were located closer to the endosteal area. The difference in porosity between periosteal and endosteal areas was mostly due to Po.Dm variations and, to a lesser extent, to Po.N. These results are concordant with previous observations in a large Australian population ranging in age from 20 to 97 years old, which were acquired using a 2D analysis of microradiographs of the mid-shaft of the femur [42]. Indeed, they reported a progressive increase in the mean pore area from the periosteal to the endosteal layers in each age group and in both sexes [42].

Connectivity

The present study is the first to report pore network connectivity at different sites within the bone. Because the connectivity density (ConnD) was characterized by high variability, it was not possible to demonstrate any difference between sites. However, the diaphysis demonstrated low connectivity with intermediate values in the inferior neck and high values in the superior region of the femoral neck. Only a single previous study by Cooper et al. reported Po.ConnD values in the range of 2.5 to 28.5 [13]. In addition to differences in the method of calculation used, the discrepancies between their results and ours could be related to the fact that, in conventional micro-CT, artifacts related to the use of cone-beam geometry could lead to discontinuities in the pore system.

Density resolution

SR micro-CT imaging provides a more quantitative image than polychromatic cone-beam micro-CT due to the use of parallel-beam geometry. Parallel-beam CT permits an exact reconstruction in the sense that there is an exact analytic reconstruction formula relating the 3D image to its projection. Thus, SR micro-CT avoids cone-beam artifacts that derive from the acquisition geometry and beam-hardening artifacts due to the monochromaticity of the source and consequently provides quantitative images well-suited to quantification of the DMB.

There was a lower DMB in the superior neck, which is consistent with a higher remodeling rate. We did not find differences between the diaphysis and inferior femoral neck. These results, which are not concordant with those based on physical density measurements, indicated that cortical bone in the femoral neck is highly mineralized compared to that of the femoral shaft [6, 19].

With conventional micro-CT images, although it was possible to discriminate pores, border osteons and density differences between osteons, the lamellae, and cement lines could not be resolved [11, 36]. Because of the high signal-to-noise ratio and the absence of a beam-hardening effect, the reconstruction of synchrotron images is potentially advantageous for distinguishing primary and secondary osteons from interstitial bone but requires the use of a sophisticated segmentation method [43]. Nevertheless, better resolution is needed to visualize the osteon border.

Conclusion

The results of the present study provide evidence for large variations in the internal pore network structure of cortical bone experiencing different loading regimes. These variabilities are probably underestimated due to our limited sample size. The porosity is dependent on both Po.Dm and Po.N at the inferior neck and diaphysis and to a lesser extent on Po.Dm at the superior neck. There is a gradient of porosity extending from the periosteum to the endosteum that is more marked in the femoral neck than in the diaphysis. The superior region of the femoral neck has a lower DMB. Consequently, we can assume that different remodeling processes occur at these different sites.

References

1. Cummings SR, Melton LJ (2002) Epidemiology and outcomes of osteoporotic fractures. Lancet 359:1761–1767, Review
2. Holzer G, von Skrbensky G, Holzer LA, Pichl W (2009) Hip fractures and the contribution of cortical versus trabecular bone to femoral neck strength. J Bone Miner Res 24:468–474
3. Schaffler MB, Burr DB (1988) Stiffness of compact bone: effects of porosity and density. J Biomech 21:13–16
4. Martin RB, Ishida J (1989) The relative effects of collagen fiber orientation, porosity, density, and mineralization on bone strength. J Biomech 22:419–426
5. McCalden RW, McGeough JA, Barker MB, Court-Brown CM (1993) Age-related changes in the tensile properties of cortical bone. The relative importance of changes in porosity, mineralization, and microstructure. J Bone Joint Surg Am 75:1193–1205
6. Yeni YN, Norman TL (2000) Fracture toughness of human femoral neck: effect of microstructure, composition, and age. Bone 26:499–504, Erratum in: Bone 2000 27:327
7. Stout SD, Brunsden BS, Hildebolt CF, Commean PK, Smith KE, Tappen NC (1999) Computer-assisted 3D reconstruction of serial sections of cortical bone to determine the 3D structure of osteons. Calcif Tissue Int 65:280–284
8. Müller R (2009) Hierarchical microimaging of bone structure and function. Nat Rev Rheumatol 5:373–381
9. Bousson V, Peyrin F, Bergot C, Haussard M, Sautet A, Laredo J (2004) Cortical bone in the human femoral neck: three-dimensional appearance and porosity using synchrotron radiation. J Bone Miner Res 19:794–801
10. Cooper DM, Erickson B, Peele AG, Hannah K, Thomas CD, Clement JG (2011) Visualization of 3D osteon morphology by synchrotron radiation micro-CT. J Anat 219:481–489
11. Wachter NJ, Augat P, Krischak GD, Mentzel M, Kinzl L, Claes L (2001) Prediction of cortical bone porosity in vitro by microcomputed tomography. Calcif Tissue Int 68:38–42
12. Cooper DML, Turinsky AML, Jensen CW, Hallgrimsson B (2003) Quantitative 3D analysis of the canal network in cortical bone by microcomputed tomography. Anat Rec 274:169–179
13. Cooper DM, Thomas CD, Clement JG, Turinsky AL, Sensen CW, Hallgrímsson B (2007) Age-dependent change in the 3D structure of cortical porosity at the human femoral midshaft. Bone 40:957–965
14. Cooper D, Turinsky A, Sensen C, Hallgrimsson B (2007) Effect of voxel size on 3D micro-CT analysis of cortical bone porosity. Calcif Tissue Int 80:211–219
15. Basillais A, Bensamoun S, Chappard C, Brunet-Imbault B, Lemineur G, Ilharreborde B, Ho Ba Tho M, Benhamou C (2007)

Three-dimensional characterization of cortical bone microstructure by microcomputed tomography: validation with ultrasonic and microscopic measurements. J Orthop Sci 12:141–148

16. Chen H, Zhou X, Shoumura S, Emura S, Bunai Y (2010) Age- and gender-dependent changes in three-dimensional microstructure of cortical and trabecular bone at the human femoral neck. Osteoporos Int 21:627–636

17. Zebaze RM, Ghasem-Zadeh A, Bohte A, Iuliano-Burns S, Mirams M, Price RI, Mackie EJ, Seeman E (2010) Intracortical remodelling and porosity in the distal radius and post-mortem femurs of women: a cross-sectional study. Lancet 15:1729–1736

18. Currey JD (2002) Bone: structure and mechanics. Chapter 1. Princeton University Press, Princeton

19. Brown CU, Yeni YN, Norman TL (1998) Fracture toughness of the femoral neck, femoral shaft, and tibial shaft in aged bone. Adv Bioeng 39:279–280

20. Lotz JC, Cheal EJ, Hayes WC (1995) Stress distributions within the proximal femur during gait and falls: implications for osteoporotic fracture. Osteoporos Int 5:252–261

21. Mayhew PM, Thomas CD, Clement JG, Loveridge N, Beck TJ, Bonfield W, Burgoyne CJ, Reeve J (2005) Relation between age, femoral neck cortical stability, and hip fracture risk. Lancet 366:129–135

22. Nuzzo S, Peyrin F, Cloetens P, Baruchel J, Boivin G (2002) Quantification of the degree of mineralization of bone in three dimensions using synchrotron radiation microtomography. Med Phys 29:2672–2681

23. Chappard C, Basillais A, Benhamou L, Bonassie A, Brunet-Imbault B, Bonnet N, Peyrin F (2006) Comparison of synchrotron radiation and conventional x-ray microcomputed tomography for assessing trabecular bone microarchitecture of human femoral heads. Med Phys 33:3568–3577

24. Salome M, Peyrin F, Cloetens P, Odet C, Laval-Jeantet AM, Baruchel J, Spanne P (1999) A synchrotron radiation microtomography system for the analysis of trabecular bone samples. Med Phys 26:2194–2204

25. Hildebrand T (1997) A new method for the model independent assessment of thickness in three dimensional images. J Microsc 185:67–75

26. Lorensen WE, Cline HE (1988) Marching cubes: a high resolution 3D surface construction algorithm. Comput Graph 21(Suppl 1):7–12

27. Ulrich D, Van Rietbergen B, Laib A, Ruegsegger P (1999) The ability of three dimensional structural indices to reflect mechanical aspects of trabecular bone. Bone 25:55–60

28. Whitehouse WJ (1974) The quantitative morphology of anisotropic trabecular bone. J Microsc 101:153–156

29. Odgaard A (1997) Three-dimensional methods for quantification of cancellous bone architecture. Bone 20:315–328

30. Odgaard A, Gundersen HJ (1993) Quantification of connectivity in cancellous bone, with special emphasis on 3-D reconstructions. Bone 14:173–182

31. Norman GR, Streiner DL (2000) Biostatistics: the bare essentials. BC Becker Inc

32. Cooper DM, Matyas JR, Katzenberg MA, Hallgrimsson B (2004) Comparison of microcomputed tomographic and microradiographic measurements of cortical bone porosity. Calcif Tissue Int 74:437–447

33. Peyrin F, Salome M, Nuzzo S, Cloetens P, Laval-Jeantet AM, Baruchel J (2000) Perspectives in three-dimensional analysis of bone samples using synchrotron radiation microtomography. Cell Mol Biol 46:1089–1102

34. Szulc P, Seeman E (2009) Thinking inside and outside the envelopes of bone. Osteoporos Int 20:1281–1288

35. Bell KL, Loveridge N, Power J, Garrahan N, Meggitt BF, Reeve J (1999) Regional differences in cortical porosity in the fractured femoral neck. Bone 24:57–64

36. Stein M, Feik S, Thomas C, Clement J, Wark J (1999) An automated analysis of intracortical porosity in human femoral bone across age. J Bone Miner Res 14:624–632

37. Pfeiffer S, Crowder C, Harrington L, Brown M (2006) Secondary osteon and Haversian canal dimensions as behavioral indicators. Am J Phys Anthropol 131:460–468

38. Bell KL, Loveridge N, Reeve J, Thomas CD, Feik SA, Clement JG (2001) Super-osteons (remodeling clusters) in the cortex of the femoral shaft: influence of age and gender. Anat Rec 264:378–386

39. Orwoll ES (2003) Toward an expanded understanding of the role of the periosteum in skeletal health. J Bone Miner Res 18:949–954, Review

40. Allen MR, Burr DB (2005) Human femoral neck has less cellular periosteum, and more mineralized periosteum, than femoral diaphyseal bone. Bone 36:311–316

41. Muller R, Van Campenhout H, Van Damme B, Van Der Perre G, Dequeker J, Hildebrand T, Ruegsegger P (1998) Morphometric analysis of human bone biopsies: a quantitative structural comparison of histological sections and micro-computed tomography. Bone 23:59–66

42. Thomas CD, Feik S, Clement JG (2006) Increase in pore area, and not pore density, is the main determinant in the development of porosity in human cortical bone. J Anat 209:219–230

43. Peter Z, Bousson V, Bergot C, Peyrin F (2008) A constrained region growing approach based on watershed for the segmentation of low contrast structures in bone micro-CT images. Pattern Recogn 41:2358–2368